Published in final edited form as:
Environ Sci Technol. 2011 February 15; 45(4): 1399–1406. doi:10.1021/es103324z.

Pentachlorophenol radical cations generated on Fe(III)-montmorillonite initiate octachlorodibenzo-*p*-dioxin formation in clays: DFT and FTIR studies

Cheng Gu[a], **Cun Liu**[a], **Cliff T. Johnston**[b,*], **Brian J. Teppen**[a,*], **Hui Li**[a], and **Stephen A. Boyd**[a,*]

[a] Department of Crop and Soil Sciences, Michigan State University, East Lansing, MI 48824

[b] Crop, Soil and Environmental Sciences, Purdue University, 915 W. State Street, West Lafayette, IN, 47907

Abstract

Octachlorodibenzodioxin (OCDD) forms spontaneously from pentachlorophenol (PCP) on the surfaces of Fe(III)-saturated smectite clay (1). Here, we used *in situ* FTIR methods and quantum mechanical calculations to determine the mechanism by which this reaction is initiated. As the clay was dehydrated, vibrational spectra showed new peaks that grew and then reversibly disappeared as the clay rehydrated. First principle DFT calculations of hydrated Fe-PCP clusters reproduced these transient FTIR peaks when inner-sphere complexation and concomitant electron transfer produced Fe(II) and PCP radical cations. Thus, our experimental (FTIR) and theoretical (quantum mechanical) results mutually support the hypothesis that OCDD formation on Fe-smectite surfaces is initiated by the reversible formation of metastable PCP radical cations via single electron transfer from PCP to Fe(III). The negatively charged clay surface apparently selects for this reaction mechanism by stabilizing PCP radical cations.

Keywords

octachlorodibenzo-*p*-dioxin; radical cation; montmorillonite; pentachlorophenol; FTIR; DFT

Introduction

Polychlorinated dibenzo-*p*-dioxins (PCDDs) and furans (PCDFs) are formed and found as a group of chlorinated congeners generated as by-products of human activities, such as waste incineration, metal smelting, and pesticide manufacture, and by natural processes such as forest fires. Each of these known sources produces a mixture of PCDDs distinguishable by their congener profiles. However, recent studies have reported high levels of PCDDs in otherwise pristine soils and pre-industrial clay deposits, with a typical congener profile characterized by the predominance of octachlorodibenzodioxin (OCDD) and low levels of PCDFs, which does not match any known anthropogenic or natural source (2–4). Global PCDD budgets fail to account for the observed levels of these compounds in soils, and OCDD presents the greatest imbalance (5). Based on bulk radiocarbon, compound-specific

*To whom correspondence should be addressed. Cliff T. Johnston, Phone: (765) 496-1716, Fax: (765) 496-2926, clays@purdue.edu. Brian J. Teppen, Phone: (517) 355-0271 ext. 254, Fax: (517) 355-0270, teppen@msu.edu. Stephen A. Boyd, Phone: (517) 881-0579, Fax: (517) 355-0270, boyds@msu.edu.

Supporting Information Available
Additional experimental data and modeling. This material is available free of charge via the Internet at http://pubs.acs.org.

chlorine isotope and black carbon analysis, Holmstrand et al. (3) proposed that the unusual congener profile of PCDDs in a ball clay deposit from the Mississippi Embayment could result from *in situ* clay mineral-facilitated synthesis of PCDDs. Congener-specific carbon isotopic analysis showed that the carbon isotope composition of OCDD found in ball clays was significantly different from known anthropogenic OCDD, further supporting the hypothesis of natural PCDD formation mechanism(s) on clay surfaces (4). The use of ball clays as animal feed additives has led to several instances of livestock contamination with PCDDs (6). A recent survey of PCDD/PCDF levels among a population living on or near dioxin-contaminated floodplain soils in Midland, Michigan revealed that the individual with the highest body burden was a potter who had a history of firing ball clays in an in-home unvented kiln (7). These examples document the potential for dioxin exposure directly related to PCDD contaminated clays.

Recently we provided the first direct evidence showing that OCDD can be formed on the clay mineral montmorillonite, under environmentally relevant conditions (1). Montmorillonite is a member of the smectite group of 2:1 aluminosilicate clay minerals, which occur naturally and are widely distributed in soils/subsoils, sediments, and geologic clay deposits (8). Negative charges embedded in the aluminosilicate layers due to isomorphous substitution are balanced by inorganic cations commonly found in nature, e.g., Ca^{2+}, Na^{+}, Mg^{2+}, and Fe^{3+} among others. The aluminosilicate layers of smectites are planar with aspect ratios of ~500 manifesting high surface areas of ~800 $m^2\ g^{-1}$. Smectite clays commonly occur as assemblages of stacked clay layers, resulting in large amounts of internal, interlayer surface where the exchangeable inorganic cations and water reside.

When the precursor molecule pentachlorophenol (PCP) was mixed with homoionic Fe(III)-montmorillonite at room temperature, OCDD rapidly formed at environmentally relevant levels (1). We proposed that the reaction was initiated by one electron transfer from PCP to Fe(III)-montmorillonite to form the PCP radical cation, followed by dimerization, dechlorination, and ring closure reactions (1, 9–11). Formation of the reactive PCP radical cation would then be the crucial step that initiates the proposed reaction pathway to OCDD. Accordingly, we hypothesized that the PCP radical cation was stabilized by the planar negatively charged smectite clay layers. By comparison, hydrated transition metal ions in aqueous solution are incapable of inducing the electron transfer so that the radical cation species is not formed, indicating the unique role played by the planar silicate surface (10). The electron transfer reaction is influenced by the presence of water, as the organic molecules must compete with water for the coordination sites of the metal cation (1). Thus, yields of OCDD from the Fe(III)-montmorillonite catalyzed reaction were inversely related to the relative humidity (RH) of the system (1). However, anhydrous conditions were not required for the reaction to proceed. Formation of organic radicals on smectites have been observed by various techniques, such as electron spin resonance (ESR) (9, 10), Fourier transform infrared (FTIR) (12) and resonance Raman spectroscopy (13, 14). Johnston et al. (15, 16) used FTIR to monitor *in situ* chemisorption of *p*-dimethoxybenzene on Cu-smectite clay. Concomitant with a decrease in RH, several IR vibrational modes were significantly perturbed and new peaks were observed, which were attributed to the formation of radical cations (15, 16). The reduction of transitional metals in the interlayer was also confirmed by ESR (9) and direct measurements (11).

Recently, first principle calculations based on density functional theory (DFT), using both cluster models and periodic boundary conditions, have been applied to studies of clay or hydrated clay structural properties (17,18), and clay mineral adsorption/catalytic reactions involving organic molecules (19–22). Cluster models have proven to provide accurate geometric and electronic structures of transition metals interacting with organics, at modest computational costs (23–25). Due to constraints in computational resources, in the current

study a cluster model of hydrated Fe(III) complexed with PCP was applied to investigate the electronic/spectroscopic properties of interlayer Fe(III)/PCP complexes. The choice of the hydrated iron cation model was based on the observation that in Fe-smectites and low-Fe-zeolites the dominant Fe(III) species identified by Mossbauer and EXAFS studies were isolated $Fe(OH)^{2+}$ or $Fe(OH)_2^{+}$ octahedrally coordinated by water (26–28). Also, ESR has been used to show that partial dehydration of iron-exchanged zeolites (achieved by applying vacuum or heat) results in removal of water molecules from Fe(III) hydration shells, and a reduced coordination number around Fe(III) (29). Since the observed Fe-catalyzed dimerization of PCP was sensitive to clay hydration (1), calculations of gas-phase PCP/$Fe(OH)(H_2O)_n^{2+}$ with various numbers of water molecules in the first hydration shell (n=0 to 3) were selected as feasible structural models to characterize the electronic (and hence spectroscopic) features of PCP radical formation in Fe(III)-smectite. While gas-phase $Fe(OH)(H_2O)_n^{2+}$ is the simplest model for hydrolyzed Fe in the interlayer, it may overestimate Fe reactivity compared with the more networked Fe expected in smectite interlayers.

The objective of this study was to couple spectroscopic evidence with quantum mechanical calculations to investigate the critical step that initiates the proposed OCDD formation mechanism (1). We hypothesize that the reaction is initiated via a one electron transfer from PCP to Fe(III) of Fe(III)-montmorillonite to form the central reactive intermediate, i.e., the PCP radical cation, which is favored by stabilization effects of the clay surface. The surface IR spectra were collected *in situ* in a controlled humidity IR cell to correlate formation of the putative PCP radical cation with changes in the vibrational spectra as a function of water content in the system. Quantum mechanical calculations on the reaction of PCP with Fe(III)-montmorillonite clay using different levels of models were conducted in concert and compared with experimental FTIR data. The theoretical and experimental results were found to be mutually consistent.

Materials and Methods

Preparation of Self-supporting Clay films

Details on the preparation of Fe(III)-montmorillonite and self-supporting clay films are included in the supporting information (SI).

In Situ FTIR Analysis

Infrared spectra were obtained on a Perkin-Elmer GX2000 FTIR spectrometer equipped with deuterated triglycine and mercury-cadmium-telluride detectors, and a KBr beam splitter. A self-supporting clay film was mounted in a vacuum cell, which was connected to a gas/vacuum manifold to control and monitor the pressure in the cell. The unapodized resolution for the FTIR spectra was 2.0 cm^{-1}, and a total of 64 scans were collected for each spectrum.

Dehydration of the clay films was accomplished by placing the films under vacuum, and the surface reactions were monitored *in situ* using the FTIR spectrometer. After the system stabilized (approximately 2 h), the vacuum was removed, a drop of water was added to the cell, and FTIR spectra were collected until a new equilibrium was achieved, as indicated by no further change in spectra. To estimate the water content on the clay film, the FTIR absorptivity of the HOH bending band at 1630cm^{-1} was determined by integrating the area of the band.

Computational Methods

In this study, DFT methods were applied to investigate the electronic and vibrational spectroscopic features associated with interactions between PCP and clay interlayer Fe(III) during dehydration/hydration cycles by modeling interlayer Fe(III) as $Fe(OH)(H_2O)_n^{2+}$ (n=0 to 3). The total coordination number of the Fe(III) center, including coordinated H_2O and PCP, ranged from two to six. The geometries of all complexes in the gas phase were fully optimized using the Becke three-parameter exchange functional (B3) (30) and the Lee–Yang–Parr correlation functional (LYP) (31), implemented in the Gaussian 03 package (32), followed by calculations of harmonic vibrational frequencies. The LANL2DZ basis set with effective core potentials (ECP) was used for Fe, while the 6–31G* basis set was used for all other atoms in the $PCP/Fe(OH)(H_2O)_n^{2+}$ complexes. Combining B3LYP methods and LANL2DZ ECPs has been found to produce reasonably accurate vibrational frequencies for a wide range of transition-metal complexes (33). The numbering scheme used for PCP atoms is shown in SI 1. A scaling factor of 0.98 was used to compare the computed frequencies with experimental data in the present study based on previous literature (34). Further normal mode decomposition analysis was carried out to interpret the vibrational spectra and peak shifts, and thereby infer the initial steps in the reaction mechanism for clay-catalyzed conversion of PCP to OCDD. Additional computations on interactions between PCP species and model clay surfaces are included in SI.

Results and Discussion

FTIR Analysis

Several *in situ* FTIR spectra of the Fe(III) montmorillonite-PCP system (Fe(III)-Swy2/PCP) are shown in Figure 1. Since clays strongly absorb infrared (IR) radiation below frequencies of 1250 cm^{-1}, and most PCP vibrational bands except the OH-stretching mode ν(OH) occur below 1700 cm^{-1}, the IR data in the 1250–1700 cm^{-1} region are displayed. The spectrum (Figure 1a) corresponding to the Fe(III)-Swy2/PCP clay film exposed to ambient air displayed peaks at 1278, 1381 and 1420 cm^{-1}, which are assigned to the combination of benzene ring breathing and C-OH stretching ν(C-OH) and bending δ(C-OH) modes (35, 36). The 1631 cm^{-1} peak (Figure 1a) corresponds to the HOH angle bending δ(HOH) of water present on clay surface (15,16).

As vacuum was applied, the intensity of the δ(O-H) water band diminished (Figure 1a–d and SI 2), indicating dehydration of the clay. Also, the peak at 1420 cm^{-1} shifted to 1411 cm^{-1}, and peaks at 1278 and 1381 cm^{-1} shifted to 1288 and 1385 cm^{-1}, respectively, indicating the dehydration of PCP (as discussed below). Importantly, as the clay film was dried two new peaks at 1360 and 1334 cm^{-1} appeared (Figure 1b–e and SI 2) which are attributed to the main ring-breathing peaks for the PCP radical cation (as discussed below in DFT calculations). They have shifted to a lower frequency ~50 cm^{-1} compared to molecular PCP because loss of an electron weakens C-C bonds within the ring. The FTIR spectra strongly support radical cation formation on Fe(III)-montmorillonite surface as evidenced by the peaks at 1360 and 1334 cm^{-1} and their response to water. Formation of the PCP radical cation via one electron transfer from PCP to Fe(III) of Fe(III)-smectite has been proposed as the critical step that initiates the clay-facilitated synthesis of OCDD (1, 10), and the reaction yield is known to be sensitive to the water content of the clay (1). Accordingly, a prerequisite for the proposed one electron transfer is inner sphere complexation of PCP, which requires prior removal of some waters of hydration from Fe(III). The PCP radical cation thus formed is plausibly stabilized by the negatively charged clay surface, which is also supported by the calculations on PCP/PCP radicals interacting with clay surface (See detailed discussion in SI).

A reversal of these changes in the FTIR spectra occurred as the vacuum was released and the system was again exposed to water vapor. As shown in Figure 1f, after 2 min exposure to water vapor, the water peak (1631 cm^{-1}) was restored and the peaks at 1288, 1385 and 1411 cm^{-1} all shifted back to their original positions. Additionally, the two new peaks at 1360 and 1334 cm^{-1} disappeared. Upon further exposure of the clay/PCP complex to water vapor, the water peak continued to increase in intensity, while little further change occurred for the other peaks (Figure 1f–i).

To quantify the relation between water content and radical cation formation, the peaks at 1630, 1360 and 1334 cm^{-1} were integrated and plotted as a function of exposure time to vacuum and to water vapor (SI 2). It is clearly shown that dehydration of clay, indicated by a decrease in the 1630 cm^{-1} band, promoted the formation of radical cations as indicated by the appearance and increase in the intensity of the 1360 and 1334 cm^{-1} bands. The apparent radical cation formation reaction was reversible; as the clay was rehydrated the 1360 and 1334 cm^{-1} bands diminished rapidly, indicating loss of the radical cation species. This interpretation of the FTIR results is supported by theoretical calculations presented below.

DFT Calculations

To further understand the IR spectral peak shifts that occurred upon exposure of the FeSWy-2/PCP clay film to vacuum, theoretical spectra of proposed PCP complexes were calculated and compared with the experimental results. The optimized geometries of the gas-phase systems PCP, PCP/H_2O, and PCP/$Fe(OH)(H_2O)_n^{2+}$ are shown in SI 3, and selected optimized structural parameters are presented in Table 1.

Due to the size and complexity of PCP/$Fe(OH)(H_2O)_n^{2+}$, and limitations in computing resources, it was not possible to fully calculate the potential energy profile and locate all energy minima for each complex (SI 4). Instead, geometry optimizations were performed within the low-energy regions where iron directly contacted the PCP hydroxyl group and all water molecules were in the first hydration shell of iron. Such structural configurations were confirmed to have the lowest energies in a previous study (25).

Among the optimized structures in the present study, complexes 0a, 1a, 2a and 3a (SI 3) all featured similar structural characteristics in that both O_1 and Cl_5 of the PCP molecule coordinate the iron center as a bidentate ligand, and the hydroxyl group of $Fe(OH)(H_2O)_n^{2+}$ is located opposite the position at which O_1 of PCP coordinates the Fe center (the angle of O_1-Fe-OH ranges from 138° to 163°). These four complexes generally have the lowest energies (SI 5) for their respective water contents, apparently due to stabilization of the 2σ bonding orbital ($d_z^2+p_z$) for each complex. When O_1-Fe-OH is roughly collinear, this geometry allows strong overlap of p_z orbitals from these two oxygens with the two lobes of the iron d_z^2 orbital (SI 6).

Some configurations in which PCP forms outer-sphere hydrogen bonds with $Fe(OH)(H_2O)_n^{2+}$ (e.g., complexes 3c and 1d of SI 3) have even lower energies (SI 5), but these complexes are intermediates on a different reaction path toward the low-energy phenoxy radical. They would rapidly convert into the phenoxy radical, which is proposed as the major pathway in the gas phase (37), but apparently do not do so in the clay interlayer, plausibly because of the favorable electrostatic interactions afforded to the radical cation by the negative energy field of the clay mineral (15, 18, 38). Also, their simulated IR spectra do not match with the experimental data (SI 7). Thus, despite the somewhat lower energy of the phenoxy-radical complex in the gas phase, the radical-cation reaction pathway seems to be selected in the clay. Therefore, the series of ‘a’ complexes (SI 3) was the focal point of the current study.

In the simplest PCP/Fe(OH)$(H_2O)_n^{2+}$ complex that we studied, PCP/$FeOH^{2+}$ (structure 0a of SI 3), PCP is coplanar with the $FeOH^{2+}$ cation and the Fe-O_1 and Fe-Cl_5 bond lengths are 2.173 and 2.653 Å, respectively (Table 1). The complexation increases the lengths of the O_1-H_1 and C_1-O_1 bonds, but dramatically increases the C–C bond lengths that are opposite the phenol position (C_3–C_4 and C_4–C_5, Table 1) from 1.402~1.407 Å to 1.439 Å and 1.461 Å. This effect is due to the extraction by Fe of one π electron from the benzene ring, which causes weakening of the C-C bonds (39). Thus, the PCP radical cation is formed automatically as PCP complexes with $FeOH^{2+}$, while the precomplex (that is, a complex in the absence of electron transfer) cannot be located in this study due to the negligible energy barrier between the radical cation complex and the precomplex. The reversibility of radical cation complex formation that we observed by FTIR (Figure 1) implies that this energy barrier is small in both directions.

As the coordination number of iron increases from 3 to 6 when water molecules are added into the iron hydration shell (structures 1a, 2a, 3a of SI 3), the C_3–C_4 and C_4–C_5 bond lengths of PCP gradually decrease to 1.42 Å and 1.428 Å (Table 1) in the octahedrally coordinated PCP/Fe(OH)$(H_2O)_3^{2+}$ (structure 3a of SI 3). This weakening of the C-C bonds is still profound and the PCP radical cation is formed automatically in all cases. However, the radical cation character of PCP is less pronounced as hydration increases, which is in excellent agreement with the lower yields observed experimentally (1), and the FTIR results showing that as the water content increased, radical cation bands diminished (SI 2).

The spin density on the PCP molecule in each PCP/Fe(OH)$(H_2O)_n^{2+}$ complex was calculated by natural population analysis (NPA) (Table 1). For the simplest PCP/$FeOH^{2+}$ complex (structure 0a of SI 3), an excess positive spin density of 1.04 is spread over the PCP molecule. One electron has been transferred from a π orbital of PCP to the nonbonding $\delta_{x^2-y^2}$ orbital of the iron center (as shown in SI 6) and the iron has been reduced from Fe(III) to Fe(II) (Table 1). When water molecules were sequentially added into the iron hydration shell (structures 1a, 2a, 3a of SI 3), the spin density on PCP decreased from 1.04 to 0.74 to 0.46, due to spin delocalization to the ligand water molecules (Table 1). Although these model PCP/Fe(OH)$(H_2O)_n^{2+}$ complexes lack any interaction with clay mineral surfaces, the calculations do yield changes in both PCP structure and electron density that support the hypothesized PCP radical cation formation (1), and also reproduce the correct trend of hydration effects on the radical cation formation. Furthermore, these first principle calculations help explain the spectroscopic features of the radical cation complex, as shown below.

Adding more water into the system would presumably cause displacement of PCP from the inner-sphere coordination sites of iron, due to the stronger binding affinity of water (40). Therefore, we hypothesized that the properties of PCP adsorbed on clay minerals at high water content might be simulated by the simplest PCP/water complex. Optimization of the PCP/water geometry (SI 3) shows a strong hydrogen bond between H_1 and the water oxygen, with a bond length of 1.79 Å (Table 1). In this case the distance between the PCP donor oxygen and the water receptor oxygen is 2.70 Å. The O_1-H_1 bond is elongated from 0.974 Å (for isolated PCP) to 0.990 Å for the complex, while the C_1-O_1 bond is shortened from 1.347 Å (in isolated PCP) to 1.335 Å (Table 1). The hydroxyl group of PCP tilts slightly (0.17 degree) out of the aromatic molecular plane, and the C_1-O_1-H_1 angle increases from 109.0 degree to 115.1 degree (Table 1). These significant changes in the geometries induced by hydrogen bonding would be expected to cause vibrational peak shifts, especially for the modes involved C-O-H bending and C-O stretching, as we observed for the 1411cm^{-1} δ(C-OH) and 1385 cm^{-1} ν(C-OH).

The calculated infrared spectral patterns for PCP, PCP/H_2O, and PCP/$Fe(OH)^{2+}$ (structure 0a of SI 3) are compared with the observed spectra in Figure 2. Three frequencies in the experimental spectra of PCP-clay show pronounced shifts in the presence of H_2O vapor versus vacuum, and are labeled 1, 2, and 3 in Figure 2. These modes are all dominated by ring breathing, C_1-O_1 stretching, and C_1-O_1-H_1 bending, according to their potential energy decompositions (PED) (Table 2). Due to the strong hydrogen bonding between O_1 of PCP and water, the calculated peak of 1381.3 cm^{-1} in the absence of water red-shifts 5.9 cm^{-1} toward lower frequencies for the PCP/H_2O complex (Figure 2d), and the peak at 1426.8 cm^{-1} (dry) exhibits a 15.9 cm^{-1} blue shift when hydrated, compared to calculated peak positions in the absence of water (Figure 2e). All these shifts are in good agreement with the magnitudes and directions of the corresponding experimental shifts (−4, 9, and 10 cm^{-1}, respectively, from comparison of Figure 1e versus 1i).

The appearance of computed vibrational peaks at 1357 and 1343 cm^{-1} (lines 3 and 4 of Figure 2c) for the radical cation PCP/$Fe(OH)^{2+}$ complex (structure 0a of SI 3) agrees well with the experimental spectrum (Figures 1e, 2b and SI 2). This provides strong independent support for the hypothesis that the new peaks in the experimental spectrum (Figures 1e and 2b) emanate directly from the formation of PCP radical cations. For the radical cation with its longer and weaker C-C bonds (as described above), it is expected that the ring-breathing C-C vibrational modes would shift dramatically to a lower frequency. Experimentally, each peak shifted 51 cm^{-1} (1411–1360=51 and 1385–1334=51, Table 2), and the first principle models show very similar shifts (55 and 33 respectively, Table 2). The two calculated peaks are only −3 and 9 cm^{-1} wavenumbers different from the observed peaks, and are assigned as ring breathing modes according to the potential energy distribution analysis shown in Table 2. The intensities of the two peaks are significantly enhanced by factors of 3.00 and 2.78, compared with the dominant peak at 1412 cm^{-1} for the isolated PCP molecule. Based on these calculated peak area ratios and the experimental spectrum for the sample under vacuum (Figures 1e and 2b), the experimental yield of radical cations after 120 min in vacuum was approximately 3%.

This pattern of the ring-breathing C-C vibrational modes shifting to dramatically lower frequency upon radical cation formation is sustained when more water molecules are added to the first hydration shell of iron (Figure 3, left). However, as discussed above, the radical character of the PCP cation decreases somewhat with increasing hydration, and this manifests a linear decrease in the intensity of the radical cation ring-breathing mode at 1360 cm^{-1} as the $Fe(OH)^{2+}$-PCP complex becomes more hydrated (Figure 3, right). It is important to note that, compared to the 1360 cm^{-1} peak, the mode at 1334 cm^{-1} diminishes much faster with increasing hydration, which explains why the observed peak at 1334 cm^{-1} is weaker than the peak at 1360 cm^{-1}. Increasing numbers of water molecules strongly disrupt the favorable energy with which PCP binds to the Fe center (Figure 3, right) hence suppressing the electron-transfer reaction. The binding energy of PCP to the Fe-center linearly decreases as the complex becomes more hydrated.

Summary and Environmental Significance

In summary, the critical step that initiates the clay-facilitated formation of OCDD from PCP is the formation of PCP radical cations on Fe(III)-montmorillonite surfaces. This conclusion is strongly supported by independent experimental and theoretical results: (1) The *in situ* FTIR observation of new peaks at 1360 and 1334 cm^{-1} that appear (reversibly) upon dehydration, and (2) first principle DFT calculations of models for PCP/$Fe(OH)(H_2O)_n^{2+}$ complexes that reproduce the experimentally observed IR vibrational features, and demonstrate that they are a direct result of single electron transfer from PCP to Fe(III). Detailed atomic and electronic structures of PCP complexes with interlayer Fe(III) species also illuminate the role of water in the reversible formation of the PCP radical cations.

The reactive PCP radical cation described herein initiates a series of reactions that together form OCDD. Pentachlorophenol falls with rains across the world (5), and many soils contain swelling clay minerals that could catalyze the formation of OCDD from these PCP inputs. Hence the clay facilitated OCDD formation reaction could plausibly be an important ongoing environmental process.

Supplementary Material

Refer to Web version on PubMed Central for supplementary material.

Acknowledgments

This project was supported by grant P42 ES004911 from the National Institute of Environmental Health Science (NIEHS), National Institute of Health (NIH), grant MICL08425 from U.S. Department of Agriculture (USDA) and the Michigan Agricultural Experimental Station. The authors thank Randy Cygan for constructive criticism of this paper.

Literature Cited

1. Gu C, Li H, Teppen BJ, Boyd SA. Octachlorodibenzodioxin formation on Fe(III)-montmorillonite clay. Environ Sci Technol. 2008; 42:4758–4763. [PubMed: 18678002]
2. Ferrario J, Byrne C, Cleverly D. 2,3,7,8-dibenzo-p-dioxins in mined clay products from the United States: Evidence for possible natural origin. Environ Sci Technol. 2000; 34:4524–4532.
3. Holmstrand H, Gadomski D, Mandalakis M, Tysklind M, Irvine R, Andersson P, Gustafsson O. Origin of PCDDs in ball clay assessed with compound-specific chlorine isotope analysis and radiocarbon dating. Environ Sci Technol. 2006; 40:3730–3735. [PubMed: 16830534]
4. Horii Y, van Bavel B, Kannan K, Petrick G, Nachtigall K, Yamashita N. Novel evidence for natural formation of dioxins in ball clay. Chemosphere. 2008; 70:1280–1289. [PubMed: 17825874]
5. Baker JI, Hites RA. Is combustion the major source of polychlorinated dibenzo-p-dioxins and dibenzofurans to the environment? A mass balance investigation. Environ Sci Technol. 2000; 34:2879–2886.
6. Hayward DG, Nortrup D, Gardner A, Clower M. Elevated TCDD in chicken eggs and farm-raised catfish fed a diet with ball clay from a southern United States mine. Environ Res. 1999; 81:248–256. [PubMed: 10585021]
7. Franzblau A, Hedgeman E, Chen Q, Lee SY, Adriaens P, Demond A, Garabrant D, Gillespie B, Hong B, Jolliet O, Lepkowski J, Luksemburg W, Maier M, Wenger Y. Human exposure to dioxins from clay. Environ Health Perspect. 2008; 116:238–242. [PubMed: 18288324]
8. Allen, BL.; Hajek, BF. Mineral occurrence in soil environments. In: Dixon, JB.; Weed, SB., editors. Minerals in Soil Environments. 2. Soil Science Society of America; Madison, WI: 1989. p. 199-278.
9. Boyd SA, Mortland MM. Dioxin radical formation and polymerization on Cu(II)-smectite. Nature. 1985; 316:532–535.
10. Boyd SA, Mortland MM. Radical formation and polymerization of chlorophenols and chloroanisole on copper(II)-smectite. Environ Sci Technol. 1986; 20:1056–1058. [PubMed: 22257409]
11. Liyanapatirana C, Gwaltney SR, Xia K. Transformation of triclosan by Fe(III)-saturated montmorillonite. Environ Sci Technol. 2010; 44:668–674. [PubMed: 20000674]
12. Hinedi ZR, Johnston CT, Erickson C. Chemisorption of benzene on Cu-montmorillonite as characterized by FTIR and 13C MAS NMR. Clays Clay Miner. 1993; 41:87–94.
13. Soma Y, Soma M, Harada I. Reactions of aromatic molecules in the interlayer of transition-metal ion-exchanged montmorillonite studied by resonance Raman spectroscopy. 2. Monosubstituted benzenes and 4,4′-substituted biphenyls. J Phys Chem. 1985; 89:738–742.
14. Soma YSM, Harada I. The oxidative polymerization of aromatic molecules in the interlayer of montmorillonites studied by resonance Raman spectroscopy. J Contam Hydrol. 1986; 1:95–106.

15. Johnston CT, Sposito G, Erickson C. Vibrational probe studies of water interactions with montmorillonite. Clays Clay Miner. 1992; 40:722–730.
16. Johnston CT, Tipton T, Stone DA, Erickson C, Trabue SL. Chemisorption of p-dimethoxybenzene on copper-montmorillonite. Langmuir. 1991; 7:289–296.
17. Skipper NT, Refson K, McConnell JDC. Computer simulation of interlayer water in 2:1 clays. J Chem Phys. 1991; 94:7434–7445.
18. Cygan RT, Greathouse JA, Heinz H, Kalinichev AJ. Molecular models and simulations of layered materials. J Mater Chem. 2009; 19:2470–2481.
19. Chatterjee A, Ebina T, Iwasaki T, Mizukami F. Intermolecular reactivity study to scale adsorption property of para- and meta-substituted nitrobenzene over 2:1 dioctahedral smectite. J Chem Phys. 2003; 118:10212–10220.
20. Gorb L, Lutchyn R, Zub Yu, Leszczynska D, Leszczynski J. The origin of the interaction of 1,3,5-trinitrobenzene with siloxane surface of clay minerals. J Mol Struct. 2006; 766:151–157.
21. Teppen BJ, Yu CH, Newton SQ, Miller DM, Schäfer L. Quantum molecular dynamics simulations regarding the dechlorination of trichloro ethene in the interlayer space of the 2:1 clay mineral nontronite. J Phys Chem A. 2002; 106:5498–5503.
22. Zilberberg I, Ilchenko M, Isayev O, Gorb L, Leszczynski J. Modeling the gas-phase reduction of nitrobenzene to nitrosobenzene by iron monoxide: A density functional theory study. J Phys Chem A. 2004; 108:4878–4886.
23. Fiedler A, Schroeder D, Shaik S, Schwarz H. Electronic structures and gas-phase reactivities of cationic late-transition-metal oxides. J Am Chem Soc. 1994; 116:10734–10741.
24. Shiota Y, Yoshizawa K. Methane-to-methanol conversion by first-row transition-metal oxide ions: ScO^+, TiO^+, VO^+, CrO^+, MnO^+, FeO^+, CoO^+, NiO^+, and CuO^+ J Am Chem Soc. 2000; 122:12317–12326.
25. Sun Q, Altarawneh M, Dlugogorski BZ, Kennedy EM, Mackie JC. Catalytic effect of CuO and other transition metal oxides in formation of dioxins: theoretical investigation of reaction between 2,4,5-trichlorophenol and CuO. Environ Sci Technol. 2007; 41:5708–5715. [PubMed: 17874777]
26. Helsen JA, Goodman BA. Characterization of iron(II)-and iron(III)-exchanged montmorillonite and hectorite using the Moessbauer effect. Clay Miner. 1983; 18:117–125.
27. Wasserman SR, Soderholm L, Staub U. Effect of surface modification on the interlayer chemistry of iron in a smectite clay. Chem Mater. 1998; 10:559–566.
28. Choi SH, Wood BR, Ryder JA, Bell AT. X-ray absorption fine structure characterization of the local structure of Fe in Fe-ZSM-5. J Phys Chem B. 2003; 107:11843–11851.
29. Wloch E, Sulikowski B, Dula R, Serwicka EM. Cation environment and migration in iron-exchanged zeolite Na-Y studied by ESR. Colloids Surf A: Physicochem Eng Aspects. 1996; 115:257–265.
30. Becke AD. Density-functional thermochemistry. III. The role of exact exchange. J Chem Phys. 1993; 98:5648–5652.
31. Lee C, Yang W, Parr RG. Development of the Colle-Salvetti correlation-energy formula into a functional of the electron density. Phys Rev B. 1988; 37:785–789.
32. Frisch, MJ.; Trucks, GW.; Schlegel, HB.; Scuseria, GE.; Robb, MA.; Cheeseman, JR.; Montgomery, JA., Jr; Vreven, T.; Kudin, KN.; Burant, JC.; Millam, JM.; Iyengar, SS.; Tomasi, J.; Barone, V.; Mennucci, B.; Cossi, M.; Scalmani, G.; Rega, N.; Petersson, GA.; Nakatsuji, H.; Hada, M.; Ehara, M.; Toyota, K.; Fukuda, R.; Hasegawa, J.; Ishida, M.; Nakajima, T.; Honda, Y.; Kitao, O.; Nakai, H.; Klene, M.; Li, X.; Knox, JE.; Hratchian, HP.; Cross, JB.; Bakken, V.; Adamo, C.; Jaramillo, J.; Gomperts, R.; Stratmann, RE.; Yazyev, O.; Austin, AJ.; Cammi, R.; Pomelli, C.; Ochterski, JW.; Ayala, PY.; Morokuma, K.; Voth, GA.; Salvador, P.; Dannenberg, JJ.; Zakrzewski, VG.; Dapprich, S.; Daniels, AD.; Strain, MC.; Farkas, O.; Malick, DK.; Rabuck, AD.; Raghavachari, K.; Foresman, JB.; Ortiz, JV.; Cui, Q.; Baboul, AG.; Clifford, S.; Cioslowski, J.; Stefanov, BB.; Liu, G.; Liashenko, A.; Piskorz, P.; Komaromi, I.; Martin, RL.; Fox, DJ.; Keith, T.; Al-Laham, MA.; Peng, CY.; Nanayakkara, A.; Challacombe, M.; Gill, PMW.; Johnson, B.; Chen, W.; Wong, MW.; Gonzalez, C.; Pople, JA. Gaussian 03, revision E.01. Gaussian, Inc; Wallingford, CT: 2004.

33. Bytheway I, Wong MW. The prediction of vibrational frequencies of inorganic molecules using density functional theory. Chem Phys Lett. 1998; 282:219–226.
34. Curtiss LA, Raghavachari K, Redfern PC, Pople JA. Assessment of Gaussian-3 and density functional theories for a larger experimental test set. J Chem Phys. 2000; 112:7374–7383.
35. Czarnik-Matusewicz B, Chandra AK, Tho Nguyen M, Zeegers-Huyskens T. Theoretical and experimental (400–10,000 cm^{-1}) study of the vibrational spectrum of pentachlorophenol. J Mol Spectrosc. 1999; 195:308–316. [PubMed: 10329274]
36. Rao PVR, Rao GR. Vibrational analysis of substituted phenols: Part I. Vibrational spectra, normal coordinate analysis and transferability of force constants of some formyl-, methoxy-, formylmethoxy-, methyl- and halogeno-phenols. Spectrochim Acta Part A. 2002; 58:3039–3065.
37. Qu X, Wang H, Zhang Q, Shi X, Xu F, Wang W. Mechanistic and kinetic studies on the homogeneous gas-phase formation of PCDD/Fs from 2,4,5-trichlorophenol. Environ Sci Technol. 2009; 43:4068–4075. [PubMed: 19569332]
38. Govindaraj N, Mortland MM, Boyd SA. Single electron transfer mechanism of oxidative dechlorination of 4-chloroanisole on copper(II)-smectite. Environ Sci Technol. 1987; 21:1119–1123.
39. Qin Y, Wheeler RA. Density-functional-derived structures, spin properties, and vibrations for phenol radical cation. J Phys Chem. 1996; 100:10554–10563.
40. Fein JB. The effect of aqueous metal-chlorophenolate complexation on contaminant transport in groundwater systems. Appl Geochem. 1996; 11:735–744.

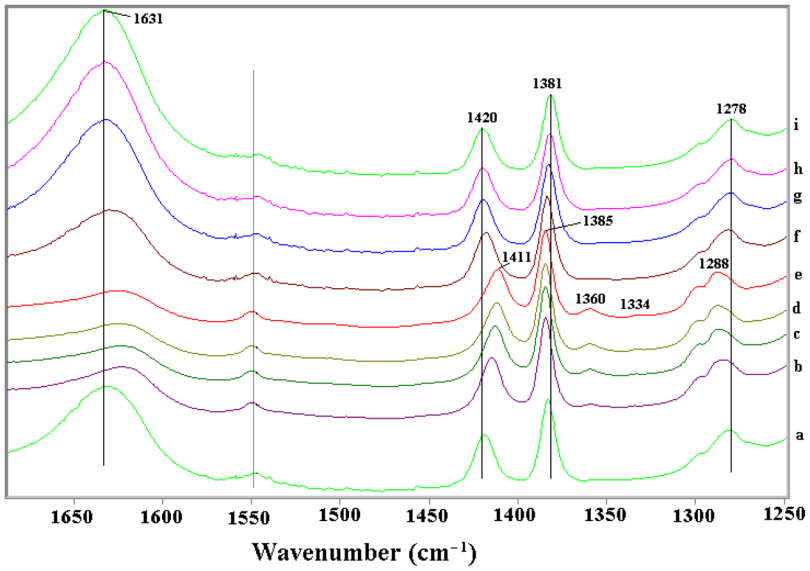

Figure 1.

FTIR spectra of homoionic Fe(III)-montmorillonite clay/pentachlorophenol self-supporting clay film exposed to vacuum as a function of time: 0 (a), 10 (b), 20 (c), 50 (d) and 120 min (e). After obtaining spectrum at t = 120 min, vacuum was closed and water was added to the cell, spectra were collected at 2 (f), 10 (g), 22 (h) and 35 (i) min after exposure to water vapor.

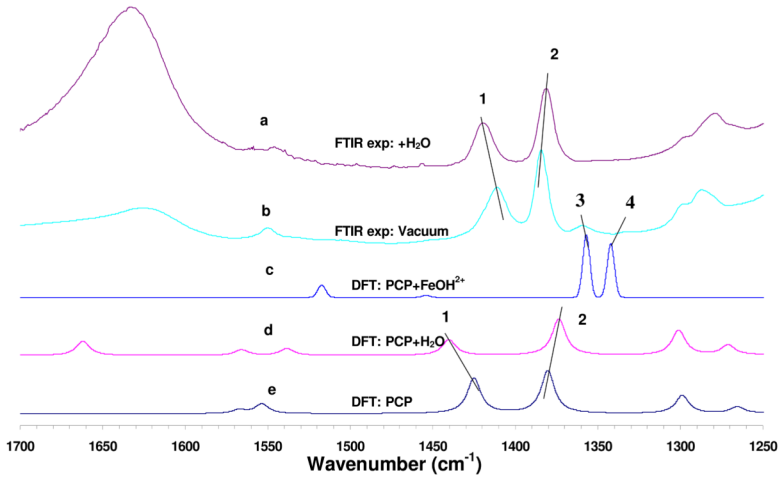

Figure 2.

Comparison of experimental infrared spectra of Fe(III)-montmorillonite clay/ pentachlorophenol (PCP) system: (a) observed spectrum after exposure to water vapor, (b) observed spectrum under vacuum, and calculated spectra (c) (d) and (e) for PCP/$FeOH^{2+}$ (structure 0a of SI 3), PCP/H_2O and PCP respectively. Lines 1, 2 indicate the peak shifts of 1420 and 1381cm^{-1}. Lines 3 and 4 indicate new peaks due to formation of radical cation in experimental (b) and calculated (c) spectra. The scaling factor was 0.98.

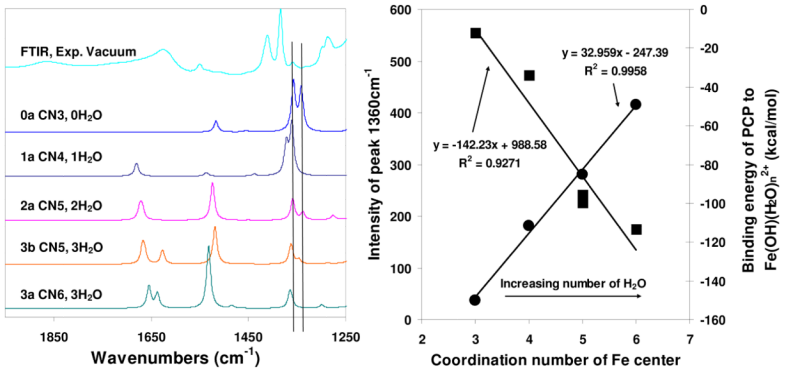

Figure 3.

Left: Calculated infrared spectra of selected PCP/$Fe(OH)(H_2O)_n^{2+}$ systems (for structures refer to SI 3) with the number of coordinated water molecules increasing from 0 to 3. Right: Correlations of intensity of the simulated infrared peak at 1360 cm^{-1} (■), and the binding energies of pentachlorophenol (PCP) onto $Fe(OH)(H_2O)_n^{2+}$ (●) versus the total coordination number of the Fe center.

Table 1

Selected computed geometrical parameters of pentachlorophenol (PCP), PCP/H_2O and PCP/$Fe(OH)(H_2O)_n^{2+}$ in the gas phase (units: distances (Å) and angles (degree))

Parameter	PCP complexes					
	PCP	PCP/H_2O	PCP/$Fe(OH)(H_2O)_n^{2+}$*			
			0a	1a	2a	3a
bond length						
C_1-O_1	1.347	1.335	1.359	1.346	1.360	1.374
O_1-H_1	0.974	0.990	0.990	0.986	0.987	0.986
C_3-C_4	1.403	1.402	1.439	1.444	1.433	1.420
C_4-C_5	1.407	1.406	1.461	1.450	1.437	1.428
H_1-O_{water}		1.793				
O_1-Fe			2.173	2.404	2.210	2.182
Fe-Cl_5			2.653	2.929	2.800	2.722
angle						
C_1-O_1-H_1	109.0	115.1	110.2	109.9	110.4	109.6
O_1-Fe-OH			162.6	138.5	138.0	162.1
dihedral angle						
benzene ring–O_1-H_1	0	0.17	0.07	0.02	4.48	0.05
spin on PCP			1.04	1.04	0.74	0.46
spin on Fe			3.58	3.61	3.73	3.84
Fe coordination number			3	4	5	6

*For structures refer to SI 3.

Environ Sci Technol. Author manuscript; available in PMC 2012 July 21.

Table 2

The calculated FTIR frequencies of all pentachlorophenol (PCP) species compared with experimental results, and the corresponding potential energy distribution analysis (PED) (percentages, in parentheses)

Species	ν_{exp} (cm^{-1})	ν_{cal} (cm^{-1})	Δ ($\nu_{cal}-\nu_{exp}$)	Assignments and %PED
PCP	1411	1426.8	+15.8	C-O str (31)+C-O-H bend (3)+ring breathing (54)
	1385	1381.3	−3.7	C-O str (3)+C-O-H bend (13)+ring breathing (65)
	1288	1301.4	+13.4	C-O-H bend (24)+ring breathing (74)
PCP/H_2O	1420	1442.7	+22.7	C-O str (1)+ring breathing (91)
	1381	1375.4	−5.6	C-O str (2)+ring breathing (83)
	1278	1302.5	+24.5	ring breathing (91)
PCP/$FeOH^{2+}$ (0a)*	1360	1357.3	−2.7	ring breathing (82)
	1334	1342.7	+8.7	ring breathing (84)
	n/a	1237.2	n/a	ring breathing (78)

*Structure 0a of SI 3.